Forecasting Residential Building Heating Load With An Innovative Gaussian Process Regression Method

Xiaoyu Sun

School of Digital Arts & Design, Dalian Neusoft University of Information, Dalian 116023, Liaoning, China

Corresponding author. E-mail: xiaoyucafa@163.com

Received: Mar. 03, 2024; Accepted: Jul. 02, 2024

Effectively controlling the heating load (HL) in residential buildings is a vital component of energy conservation and sustainability. This abstract presents a new methodology for predicting HL by incorporating Gaussian Process Regression (GPR) and harnessing the power of two groundbreaking optimization techniques: the Population-based Vortex Search Algorithm (PVS) and the Flow Direction Algorithms (FDA). GPR stands out as a robust machine learning algorithm renowned for its capacity to grasp intricate data relationships. Combining these mentioned optimizers with the GPR model results in a hybrid strategy that harnesses the unique advantages of each element. PVS and FDA are utilized to optimize the GPR's parameters, thereby elevating its predictive precision. The amalgamation of GPR, PVS, and FDA surpasses conventional techniques and even standalone GPR models regarding predictive precision and convergence velocity. This methodology offers a pragmatic and efficient approach to enhancing the forecast of HL in residential buildings, consequently aiding in better energy management and mitigating environmental impact. The hybrid GPPV model distinguishes itself with its exceptional accuracy when compared to alternative proposed models. Boasting a low RMSE of 1.013 and a R^2 value of 0.990 , GPPV attains the highest performance level. Furthermore, this research paves the way for the exploration of employing nature-inspired optimization techniques alongside neural networks to address a wide array of intricate challenges. The combined influence of GPR and these inventive optimizers highlights the capacity of hybrid models to tackle practical, real-world issues.

Keywords: Heating load, Gaussian Process Regression, Population-based Vortex Search Algorithm, Flow Direction Algorithms.

http://dx.doi.org/10.6180/jase.202506_28(6).0005

Nomenclature

GPR	Gaussian Process Regression	FDA	Flow Direction Algorithm	Or	Orientation
PVS	Population-based Vortex Search Algorithm	GPPV	GPR+PVS	OH′	Overall Height
GPFD	GPR+FDA	R^2	Coefficient of Determination	GAD	Glazing Area Distribution
RAE	Relative Absolute Error	RMSE	Root Mean Square Error	GA	Glazing Area
MDAPE	Median Absolute Percentage Error	ML	Machine Learning	HVAC	Heating, Ventilation, and Air Conditioning
PI	Prediction interval	MAE	Mean Square Error	HL	Heating Load
RC	Relative Compactness	SA	Surface Area	Fig.	Figure
WA	Wall Area	RA	Roof Area	Eq.	Equation

1. Introduction

Lately, there has been a notable increase in investigative efforts directed toward enhancing the energy efficiency of buildings. This growing interest due to ascribed to increasing apprehensions concerning power wastage and its enduring, adverse consequences on the ecosystem [1, 2]. Researchers have been diligently investigating methods to enhance building efficiency and diminish their ecological footprint. They acknowledge the significant impact of buildings on energy consumption and the emission of greenhouse gases [3, 4]. To attain energy conservation in buildings, it requires the formulation of a variety of strategies for effective energy management [5, 6]. A crucial aspect of shaping these strategies includes accurately forecasting energy consumption, a topic that has gained significant importance in recent years [7]. By closely monitoring changes in energy-building usage, it becomes achievable to plan precise and efficient power-conserving steps [8–10]. They pinpoint potential opportunities for energy conservation and address operational inefficiencies, thereby benefiting equally power preservation and the optimal operation of construction organizations [11]. These methods utilize predictive data to improve power efficiency, diminish waste, and guarantee the efficient functioning of building systems [12]. Exploration has exhibited that slight improvements in foretelling structure power utilization could result in significant cuts in power consumption. Accurate forecasts of energy consumption patterns enable the ability to make informed decisions and proactively manage energy consumption for optimization [13]. These measures can encompass a variety of strategies, such as modifying HVAC configurations, optimizing lighting timetables, installing energy-efficient machinery, and encouraging behavioral changes to align with energy conservation goals. These actions offer benefits not only to building managers but also to the occupants [14, 15].

Precisely forecasting the energy usage of buildings is a fundamental feature of modeling energy; however, it is usually deficient in replicating real-world results [16]. Numerous research studies have underscored the significant gap between anticipated and actual energy consumption, occasionally exceeding projections by two or even threefold. Old-style models of energy depend on manufacturing computations rooted in actual principles to evaluate the energy of building usage; a method well-suited for initial assessments [17]. Nonetheless, they face limitations in effectively capturing the intricacies of the actual environment. To overcome those constraints, arithmetical imitation methods are working for modeling power consumption in buildings. These simulations assist in tackling the difficulties related to the incorporation of models of machine learning into structure power effectiveness, methodically evaluating present investigative discoveries and constraints [18, 19].

Models of AI hold important promise in forecasting and improving the energy usage of buildings. This template makes use of historical datasets, immediate sensor data, and artificial intelligence algorithms to produce precise forecasts and supply valuable perceptions for efficient management of energy [20, 21]. Substantial progressions have occurred in the domain of energy usage projection over time. Investigators and specialists use numerous advanced methods and approaches in the direction of reliably anticipating power consumption [22, 23].

In a study by Kim and Cho [24], a neural network was introduced that combined features from both Convolutional Neural Network (CNN) and Long Short-Term Memory (LSTM) architectures. This amalgamation was customized for precise prediction of residential energy consumption, effectively harnessing spatial and temporal features to capture intricate energy consumption patterns adeptly. The experimental outcomes demonstrated the remarkable precision of the CNN-LSTM method, particularly in the domain of electrical power application, outstanding traditional predicting approaches. A customized Deep Neural Network (DNN) model for forecasting cooling and heating demands in residential buildings was presented by Roy and colleagues [25]. Subsequently, they conducted a comparative evaluation, where they compared the Deep neural network framework along with the (GPR), (MPMR) and (GBM). Based on the results, it was found that the GPR and DNN frameworks were able to predict both heating and cooling demands with the largest proportion of variability explained (VAF). Moradzadehand et al. [26] utilized MLP and SVR models to forecast Heating and Cooling Loads. The multi-layer perceptron method produced outstanding outcomes, with the highest R-amount of 0.9993 for HL prediction. Conversely, the SVR technique performed exceptionally well in predicting the cooling load, with a maximum value of R of around 0.9878.

Effective control of HL in residential buildings is critical for energy conservation and sustainability. HVAC systems account for approximately 50% of a typical household's energy consumption, making efficient HL forecasting a priority. The global energy demand for residential heating is projected to increase by 18% by 2030, driven by growing urbanization and climate change. Accurate forecasting of HL can lead to significant energy savings and reduce carbon emissions. This study introduces a novel machine learning methodology designed to achieve highly precise and optimal predictive results for HL forecasting in resi-

dential buildings. The primary objective is to enhance the performance of Gaussian Process Regression (GPR) models through a sophisticated hybridization technique. This approach integrates GPR with two advanced optimization techniques: the Population-based Vortex Search Algorithm (PVS) and the Flow Direction Algorithm (FDA). The innovative aspect of this research lies in the strategic combination of these optimizers to refine the GPR model's parameters, thereby surpassing the performance of traditional methods. This hybrid methodology leverages the distinct advantages of each optimizer—PVS's ability to explore complex solution spaces and FDA's efficiency in converging to optimal solutions. The deliberate integration of these techniques ensures a more robust and reliable forecasting model.

A thorough evaluation was conducted, comparing both the individual and hybrid configurations of the models to assess their capabilities impartially. This comprehensive assessment confirms that the hybrid GPR-PVS-FDA model consistently outperforms conventional approaches, signifying a noteworthy development in HL management predictive modeling. The practical implementation of this method is highly feasible. It can be integrated into building energy management systems for real-time HL predictions, promoting efficient energy use and cost savings. Deployable as a cloud-based solution, the model offers scalability and accessibility across various residential settings. Its adaptability to different building types and climates further extends its applicability. Additionally, the model's forecasts can be utilized by decision support systems to optimize heating operations, enhance energy management, and reduce environmental impact.

GPR is chosen for HL prediction due to its notable advantages in modeling flexibility, robust performance, and parameter optimization. GPR excels in capturing complex, non-linear relationships between inputs and outputs, crucial for accurately predicting HL variations influenced by factors such as weather and building characteristics. Additionally, GPR offers probabilistic predictions, providing not only point estimates but also measures of uncertainty, which are valuable for assessing prediction confidence and making informed energy management decisions. GPR's robustness makes it particularly effective in handling noisy and sparse data, common in HL datasets. Its adaptability allows the model to adjust to varying data distributions and scales, enhancing its suitability across different datasets and contexts. In terms of parameter optimization, In addition, GPR benefits significantly from advanced techniques including the PVS and the FDA. These methods efficiently tune the hyperparameters of the GPR model, leading to superior predictive performance compared to conventional parameter estimation approaches. This efficient hyperparameter tuning further strengthens GPR's ability to deliver precise and reliable forecasts in the context of HL prediction.

2. Materials and methodology

2.1. Materials

To facilitate the training of machine learning models, a dataset has been compiled using an extensive collection of published literature [27, 28]. In Table 1, statistical characteristics for the input variables can be found. This dataset encompasses the following parameters:

- Relative Compactness: This parameter quantifies the overall compactness of the building, directly influencing its heat retention and loss characteristics.
- Surface Area $\left(m^2\right)$: Accurately measuring the total surface area of the structure is vital for understanding its exposure to external thermal influences.
- Wall Area $\left(m^2\right)$: Precise recording of the wall area provides insights into the building's thermal insulation properties and its heat transfer capabilities.
- Roof Area $\left(m^2\right)$: Including roof area in the dataset is significant due to its role in the building's thermal equilibrium as a source of heat gain or loss.
- Overall, Height (m): The vertical dimension of the building is directly linked to its internal volume and, consequently, its HL requirements.
- Orientation: Knowledge of the building's orientation is essential for assessing solar exposure and its impact on heating demands.
- Glazing Area (%): Thorough documentation of the percentage of glazing or fenestration area within the building envelope is critical for understanding heat transfer dynamics through windows.
- Glazing Area Distribution: The spatial distribution of glazing across different facades of the building plays a pivotal role in shaping interior heat distribution patterns, necessitating meticulous documentation.

This dataset, built upon these parameters, is a valuable resource for the development of machine learning models, enabling more efficient and accurate predictions in the context of HL analysis.

Table 1. Statistical properties of the variables.

Componenet	Indicators						
	Group	Min	Max	Median	Avg	Skew	St. Dev.
RCE	Input	0.62	0.98	0.75	0.764	0.496	0.106
SA	Input	514.5	808.5	673.75	671.708	-0.125	88.086
WA	Input	245	416.5	318.5	318.5	0.534	43.626
RA	Input	110.25	220.5	183.75	176.604	-0.163	45.166
OVH	Input	3.5	7	5.25	5.25	-2.9 E-19	1.751
OR	Input	2	5	3.5	3.5	2.68 E-18	1.119
GA	Input	0	0.4	0.25	0.235	-0.060	0.133
GAD	Input	0	5	3	2.813	-0.089	1.551
Heating	Output	6.01	43.1	18.95	22.307	0.360	10.090

2.2. Gaussian Process Regression (GPR)

GPR emerges from extending linear regression. GLR constitutes a set of stochastic variables with a collective Gaussian distribution, making it a probabilistic multivariate regression technique. Consider a provided training dataset $D = \{(x_i, f_i), i = 1, \ldots, n\}$, where f_i equals $f(x_i)$, signifying the function's value at the sample x_i. The (GP), an expansion of the Gaussian probability distribution, is portrayed as follows:

$$f(x) \sim GP\left(m(x_i), k\left(x_i, x_j\right)\right) \tag{1}$$

In this context, x and $k\left(x_i, x_j\right)$ pertain to the average and covariance functions. The correlation matrix indicates the likeness between the two stochastic variables and is ascertained using a squared exponential (SE) kernel [29].

The function provided is as follows:

$$k\left(x_i, x_j\right) = \exp\left(\left\|x_i - x_j\right\|^2 / \left(2\sigma^2\right)\right) \tag{2}$$

In which σ represents the kernel width requiring optimization. The predictive purpose, denoted as f_*i, can be derived for a particular test model X_* in the following manner:

$$p(f_* \mid X_*, X, f) = N(f_* \mid \mu_*, \sigma_*) \tag{3}$$

Deger ZT and Kaya GT have presented an innovative preprint proposing a GPR-driven predictive model for the cyclic backbone curves of RC shear walls [30].

Where:

$$\mu_* = \underline{k}_*^T \cdot \left[K(X, X) + \sigma_n^2 I\right]^{-1} \underline{y} \tag{4}$$

$$\sigma_*^2 = K\left(\underline{X}_*, \underline{X}_*\right) - \underline{k}_*^T \left[K(X, X) + \sigma_n^2\right]^{-1} \underline{k}_* \tag{5}$$

2.3. Population-based Vortex Search Algorithm (PVSA)

The Vortex Search algorithm is a metaheuristic that encircles a solitary resolution and is famed for its proficient utilization abilities, allowing prompt implementation [31].

2.3.1. *Initializing*

Throughout the algorithm's establishment period, crucial governing factors are specified, encompassing the population size (*psize*), vortex size (*vsize*), cessation criteria, and mutation probability (η_m). The *psize* variable symbolizes the complete count of potential resolutions generated in one round and is evenly distributed to create *vsize*, corresponding to *psize*/2

At first, the tally of candidate solutions (CS) corresponds to the vsize quantity. Afterward, extra CSs are formed, extending from (*vsize* +1) to psize. The process halts when it attains the preset utmost figure of function assessments (*maxFEs*). In the subsequent stage, the polynomial adjustment procedure hinges on the likelihood variable (η_m). Moreover, μ_0 and q_0 are computed in the stated progression employing Eqs. (6) and (7):

$$\mu_0^i = \frac{upper_i + lower_i}{2} \tag{6}$$

$$q_0^i = \sigma_0^i = \frac{\max(upper_i) - \min(lower_i)}{2} \tag{7}$$

2.3.2. *First phase*

The process begins with a random assembly of *psize* individuals, with subsequent cycles involving vsize individuals. The midpoint μ is updated using a Gaussian distribution. Half the population follows the best midpoint, and the remaining portion undergoes a communaldriven process to adjust resolutions exceeding a set threshold.

$$s_i^t\left(x_i^t \mid \mu_t, v\right) = \left((2\pi)^d |v|\right)^{-\left(\frac{1}{2}\right) e^{\left(-1/2(x_i^t - \mu_t)^T v^{-1}(x_i^t - \mu_t)\right)}} \tag{8}$$

$$s_i\left(lower_i \vee s_i\right) upper_i \rightarrow s_i = rand \times (upper_i - lower_i) + lower_i \tag{9}$$

The original VS technique uses μ_0 indirectly to create the initial assembly. $PVSA_a$ includes μ_0 in the first cycle,

with μ_0 as the initial potential resolution in a group of *psize*-1 in contrast to $PVSA_b$, where the initial group is formed by random generation of *psize* potential resolutions.

2.3.3. Second phase

Eq. (10) computes the selection probability vector (pb) for every potential solution.

$$\begin{aligned} p_i &= csum_i / csum_{psize} \\ csum_i &= \sum_{j=1}^{i} normp_i \; and \\ normp_i &= p_i / \sum_{i=1}^{psize} p_i \; and \\ p_i &= 0.9 \times \left(\max\{\vec{f}\} - f_i \right) + 0.1 \end{aligned} \tag{10}$$

f depicts the health metric linked with the $i-th$ solution.

$\max\{f^{\rightarrow}\}$ signifies the highest well-being value amid the present assembly.

p_i symbolizes the adjusted health assessment of the $i-th$ resolution in the context of reduction.

normp illustrates the likelihoods achieved by standardizing the p values, guaranteeing their confinement in the interval from 0.5 to 1 .

In the subsequent portion of the populace, encompassing resolutions marked as CS_i where i lies within the v size +1 to psize scope, an arbitrary nearby resolution is chosen from the complete assembly. This selection procedure is steered by the prob vector. Utilizing Eq. (11), a casually picked dimension's value is adjusted to establish a fresh resolution, designated as CS_{new}.

Following this adaptation, the magnitude of the altered dimension is inspected to ascertain if it surpasses particular boundaries, as established in Eq. (12).

$$\begin{aligned} &CS_{new} = CS_{current} \; then \; CS^i_{new} \\ &= CS^i_{current} + \left(CS^i_{current} - CS^i_{neigbour} \right) \times (r - 0.5) \times 2 \end{aligned} \tag{11}$$

$$CS_{new} = \begin{cases} lower_i, & CS^i_{new} < lower_i \\ CS^i_{new}, & lower_i \le CS^i_{new} \le upper_i \\ upper_i, & CS^i_{new} > upper_i \end{cases} \tag{12}$$

A randomly selected value r between 0.5 and 1 determines the quality of the new resolution CS_{new}. If it's better than the current resolution $CS_{current}$, it replaces it. If not, a mutant resolution CS_{mutant} is created using polynomial transformation based on Eq. (13).

$$\begin{aligned} CS_{mutant} &= CS_{curren} + \delta_q \times (upper - lower) \\ \delta_q &= \begin{cases} \left[\begin{array}{c} 2r + (1-2r) \\ (1-\delta_1)^{\eta_m+1} \end{array} \right]^{\frac{1}{\eta_m+1}}, & if \; r \le 0.5 \\ 1 - \left[\begin{array}{c} 2(1-r) + 2(r-0.5) \\ (1-\delta_2)^{\eta_m+1} \end{array} \right]^{\frac{1}{\eta_m+1}}, & otherwise \end{cases} \\ \delta_1 &= \frac{CS_{current} - lower}{upper - lower} \\ \delta_2 &= \frac{upper - CS_{current}}{upper - lower} \end{aligned} \tag{13}$$

Random figures *rnd* generated in each dimension within a 0.5 to 1 range lead to further steps if *rnd* is less than η_m. A polynomial adjustment operator maintains diversity and a selection operation updates the midpoint μ with the best solution. The process continues until reaching the maximum function assessments, involving copying vsize resolutions in the initial phase and adding random data to the remaining population in the subsequent phase.

$$\begin{aligned} r_t &= \sigma_0 \times \frac{1}{x} \times \Gamma\left(x, \; a_t\right) \\ where a_t &= \frac{(MaxFEs - Fes)}{MaxFEs} \\ then if \; (a_t \le 0) \; a_t &= 0.1 \end{aligned} \tag{14}$$

2.4. Flow Direction Algorithms (FDA)

Flow direction methods typically use a 3×3 grid with a central unit and eight adjacent units to determine water distribution to recipient units [32, 33]. This research utilizes three SFD methods (specifically $D8$, Rho8, and D8 - LTD) and three MFD methods (namely FDFM, $MFD-md$, and $D\infty$) to compute the TCA.

2.4.1. SFD Algorithms

In a 3×3 grid, adjacent cells are categorized as cardinal (2, 4, 6, 8) and diagonal (1, 3, 5, 7). Flow direction algorithms determine water flow based on gradients between central and neighboring units, assuming water flows to one neighbor [34].

$$Slope_i = (z_0 - z_i) \, / L_i i = 1, 2, \ldots, 8 \tag{15}$$

In this equation, z_i represents the height of unit i, and L_i stands for the horizontal projected distance from the center of unit 0 to unit i. If the dimension of a unit is denoted as L, L_i is equivalent to L for cardinal units and $\sqrt{2L}$ for diagonal ones. Rho8 introduces a random parameter rho into Eq. (1)[34]:

$$Slope_i = rho.\,(z_0 - z_i)\,/\,L_i i = 1, 2, \ldots, 8 \tag{16}$$

The equation uses rho to determine flow direction, with different values for cardinal and diagonal units based on a stochastic parameter. $D8$ and $Rho8$ methods select the steepest gradient's direction as the recipient unit. $D8 - LTD$ divides the grid into eight triangular segments, choosing the steepest one as the drainage segment, which determines the recipient unit [35]. The transversal deviation is the shortest distance from the center of a potential unit to a line along the flow direction. The unit with the least transversal deviation is chosen as the sole recipient unit. For more details, refer to Orlandini et al. [35, 36].

2.4.2. *MFD Algorithms*

An MFD method distributes the water from the central unit to *several* (≥ 1) neighboring units within a 3×3 grid. In both $FDFM$ and $MFD - md$, all adjacent units positioned at a lower elevation than the central unit are acknowledged as recipient units. The distribution of water from the central unit to the recipient units is computed using the subsequent Eq. [37]:

$$f_i \max\left(0, \text{Slope}_i^p \cdot L_i\right) / \sum_{k=1}^{8} \max\left(0, \text{Slope}_i^p \cdot L_i\right) \tag{17}$$

In this formula, f_i represents the fraction of water assigned from unit 0 to unit i, Slope $_i$ denotes the incline of unit i computed using Eq. (1), L_i stands for the length of the operational perimeter, and p is an adjustable exponent. L_i equals $0.5L$ for fundamental units and $0.354L$ for slanting units. In FDFM [38], p remains constant (i,e.,1.1), but in $MFD - md$ [28], it's a variable that adapts according to the local slope:

$$p = 8.9 \cdot \min\left(Slope_i, 1\right) + 1.1 \tag{18}$$

$D\infty$ is also based on triangular facets. In contrast to $D8 - LTD$, $D\infty$ recognizes both the fundamental besides diagonal units of the drainage segment as recipient units when the flow direction is situated between diagonal and cardinal directions. The distribution of water from the essential unit to a recipient unit is reciprocally linked to the angular disparity between the flow direction and the midpoint of the recipient unit [39].

2.4.3. *TCA, Effective Contour Length, and SCA*

In a DEM, runoff units are determined using SFD or MFD techniques, calculating water ratios and Total Contributing Area (TCA).

3. Performance evaluators

A set of measures has been developed in this part to assess the hybrid models. These metrics provide important information about the models' performance by measuring both correlation and error. Table 2 contains the formulae for the measures used in this investigation [40].

As an alternative representation, the variables can be described in the following:

- The measured value is indicated by m_i.
- The $\bar{m}$ and $\bar{b}$ stand for the means of the observed and anticipated values, alternatively.
- b_i determines the predicted values.
- n defines the sample size.
- The $\bar{x}$ represents the dataset's predictor variable mean.

3.1. Modeling step

The proposed forecasting model for HL in residential buildings integrates GPR with two advanced optimization techniques, the PVS and the FDA. This hybrid approach aims to enhance predictive accuracy by fine-tuning the parameters of the GPR model. The model development process involves collecting and preprocessing data from various sources, including historical HL data, weather data, and building characteristics. Data preprocessing steps such as cleaning, normalization, and feature engineering are conducted to prepare the data for modeling.

Once the data is ready, the GPR model is trained using historical data, with the optimization algorithms utilized to optimize its hyperparameters. The training process is followed by validation to assess the model's performance, typically using metrics like R^2 and RMSE. The forecasting model offers multiple horizons for prediction, including short-term, medium-term, and long-term forecasting. Short-term forecasting spans from a few hours to a few days, while medium-term forecasting extends to several weeks, and long-term forecasting may cover months or even years. In practice, the model can be deployed for real-time forecasting applications, such as energy management systems in residential buildings. It can also be integrated into decision support systems to optimize heating system operations and energy usage. The model's scalability and adaptability allow it to be applied across different building types, climates, and operational conditions.

3.2. Hyperparameters

Table 3 presents the results of hyperparameters for two hybrid models of GPR: GPPV and GPFD. These models

Table 2. Formulations of the Performance Metrics.

Coefficient Correlation (R^2) :	$R^2 = \left(\frac{\sum_{i=1}^{n} (b_i - \bar{b})(m_i - \bar{m})}{\sqrt{\left[\sum_{i=1}^{n} (b_i - \bar{b})^2\right]\left[\sum_{i=1}^{n} (m_i - \bar{m})^2\right]}} \right)^2$
Root Mean Square Error (RMSE):	$RMSE = \sqrt{\frac{1}{n} \sum_{i=1}^{n} (m_i - b_i)^2}$
Mean Square Error (MSE):	$\mathrm{MSE} = \frac{1}{n} \sum_{j=1}^{n} (m_i - b_i)^2$
Median Absolute Percentage Error (MDAPE):	$MDAPE = 100 \times Md \left(\frac{m_i - b_i}{m_j} \right)$
Prediction interval (PI):	$PI = \pm t \times SE \times \sqrt{\left(1 + \frac{1}{n} + \frac{(x^* - \bar{x})^2}{\Sigma (x_i - \bar{x})^2}\right)}$

integrate GPR with different optimization techniques-PVS for GPPV and FDA for GPFD. The hyperparameters listed include n_restarts, length_scale, and alpha, which are crucial for optimizing the performance of the GPR models.

4. Result and discussion

Table 3 provides a comprehensive view of the performance of three models, GPR, GPPV, and GPFD, across different phases, including the training, validation, and test phases, as well as an overall assessment. The metrics examined in this evaluation encompass RMSE, R^2, MSE, MDAPE, and PI. In the Training Phase, GPPV outperforms GPR and GPFD in terms of RMSE, demonstrating the lowest error at 1.013.R^2 values show a high level of goodness-of-fit to the training data, with GPPV achieving the highest R^2 of 0.990 . GPPV also excels in terms of MSE and MDAPE, achieving the lowest values, while its PI is the narrowest, indicating greater precision. Moving to the Validation Phase, GPPV continues its remarkable performance with the lowest RMSE, highest R^2, and lowest MSE among the models. The MDAPE is also lower for GPPV, indicating superior performance and the PI for GPPV is the narrowest, underscoring its reliability. In the Test Phase, GPPV maintains its superior performance with the lowest RMSE, highest R^2, and lowest MSE among the models. It is worth noting that while GPPV has the lowest MDAPE, the GPR model achieves the lowest PI.

Across all phases, GPPV consistently displays the lowest RMSE, the highest R^2, and the lowest MSE, signifying its robust performance. MDAPE values remain lowest for the GPPV model, indicating its accuracy in predictions. The PI for GPPV consistently maintains a narrower range, suggesting higher precision. In summary, GPPV consistently outperforms both GPR and GPFD across all phases in terms of RMSE, R^2, MSE, MDAPE, and PI, establishing itself as the most accurate and reliable model among the three.

A scatter plot showing the models' performance in terms of R^2 and RMSE values is shown in Fig. 1. Different colored, circular markers are used to symbolize each model in training, validation, and testing phases. The markers overlap perfectly between the anticipated and actual values, converging toward a center line that represents the ideal R^2 value of 1 . A highly clustered cluster is visible close to the middle line when the data points connected to the GPPV model inside the plot are examined more carefully. The scatter plot's tight clustering of data

In contrast, dispersed data points are displayed by the GPFD and GPR models, suggesting a larger range of values. This dispersion suggests that these models have inconsistent predictions and might not always achieve high R^2 values. The scatter plot shown in Fig. 1 highlights the increased variety in the predictions provided by the GPFD and GPR models while also emphasizing the improved predictive accuracy of the GPPV model.

Table 3. The result of developed models for GPR.

Phase	Index values	Models		
		GPR	GPPV	GPFD
Train	RMSE	1.752	1.013	1.474
	R^2	0.971	0.990	0.981
	MSE	3.070	1.026	2.173
	MDAPE	6.798	3.268	3.513
	PI	0.040	0.023	0.033
Validation	RMSE	2.137	1.526	1.891
	R^2	0.957	0.976	0.965
	MSE	4.566	2.327	3.577
	MDAPE	7.207	6.363	4.259
	PI	0.050	0.036	0.044
Test	RMSE	1.857	1.192	1.604
	R^2	0.967	0.986	0.980
	MSE	3.449	1.422	2.574
	MDAPE	6.405	4.344	4.899
	PI	0.041	0.026	0.035
All	RMSE	1.831	1.132	1.563
	R^2	0.968	0.988	0.978
	MSE	3.351	1.280	2.444
	MDAPE	6.774	3.747	3.767
	PI	0.041	0.025	0.035

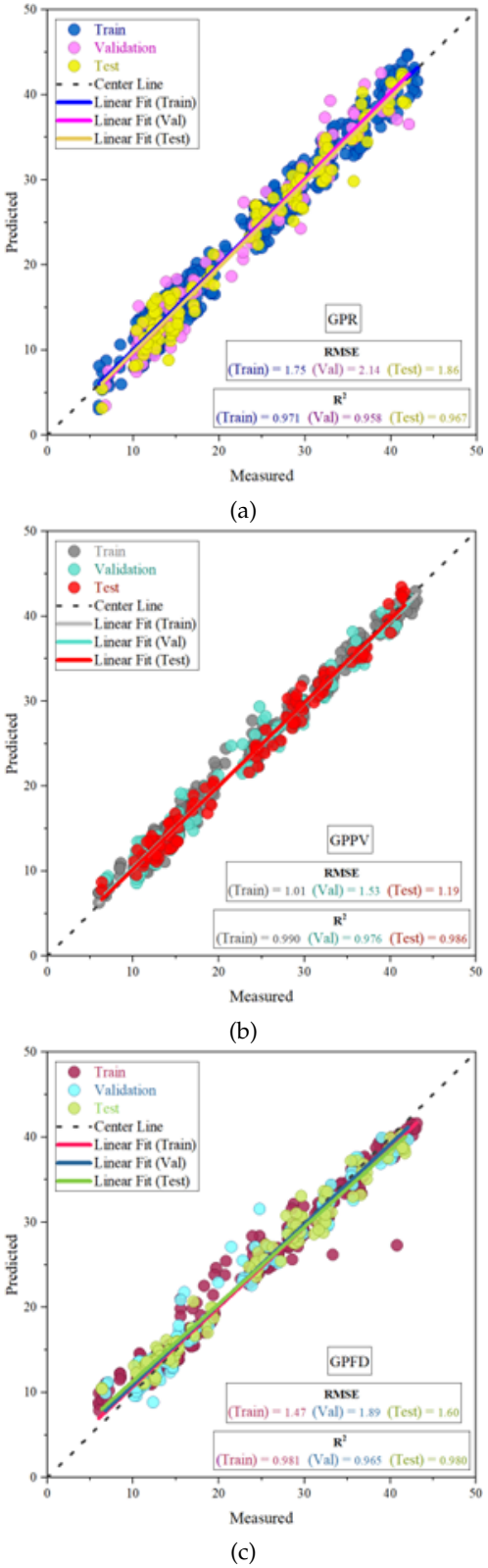

Fig. 1. Scatter plot for the developed models.

The correlation between the measured and anticipated values of the basic GPR models is shown in Fig. 2. The measured values are shown in this illustration by the solid lines. The accuracy of the model is indicated when the predicted values closely match the measured values. The data produced by the GPR model and the observed values show a clear disparity, as Fig. 2 shows, which is especially visible during the testing phase. On the other hand, the GPPV model exhibits an accurate result, showing almost complete agreement between its measured and predicted values, especially when considering sample sizes between 0 and 100 . This highlights the model's capability to predict HL with high precision and reliability.

In contrast, the GPFD model determines a conspicuous lack of accuracy, particularly within the sample numbers between 50 and 200. This divergence between the predicted and measured values positions the GPFD model as less precise than the GPPV model. It implies that the GPPV model excels in delivering more reliable and precise predictions for HL across a broader spectrum of sample numbers, whereas the GPFD model encounters some variability in its precision within specific sample number intervals.

Conducting a thorough error analysis is imperative for achieving a deeper comprehension of the unique characteristics and precision of the models under investigation. This analysis enables us to explore the intricacies of their performance. Fig. 2 is a crucial reference point in this pursuit, providing insights into the models' performance regarding errors. Notably, the GPR model, as emphasized by the graph, exhibited a significant error rate, especially prominent during the testing phase. The highest error, reaching up to 40%, was particularly conspicuous within the sample range from 500 to 650 . This observation underscores the difficulties faced by the GPR model, especially in accurately predicting HL values within this specific sample range.

Converselymore thorough examination of the GPPV model demonstrates an extraordinary degree of accuracy throughout the training phase, with most data points displaying errors that were almost minor and remained close to 0%. This suggests that during the training phase, the GPPV model performs exceptionally well in predicting HL values. But as testing progresses, a somewhat different picture emerges - some flaws show up, but they are comparatively less than those found in the GPR model. On the other hand, the GPFD model's performance demonstrates unique features. It registered a 50% peak error during the training period, demonstrating some degree of irregularity in its predicting accuracy. Notably, these mistakes continue throughout the training, testing, and validation stages, highlighting its distinct behavior even more.

The distribution properties of the proposed models are

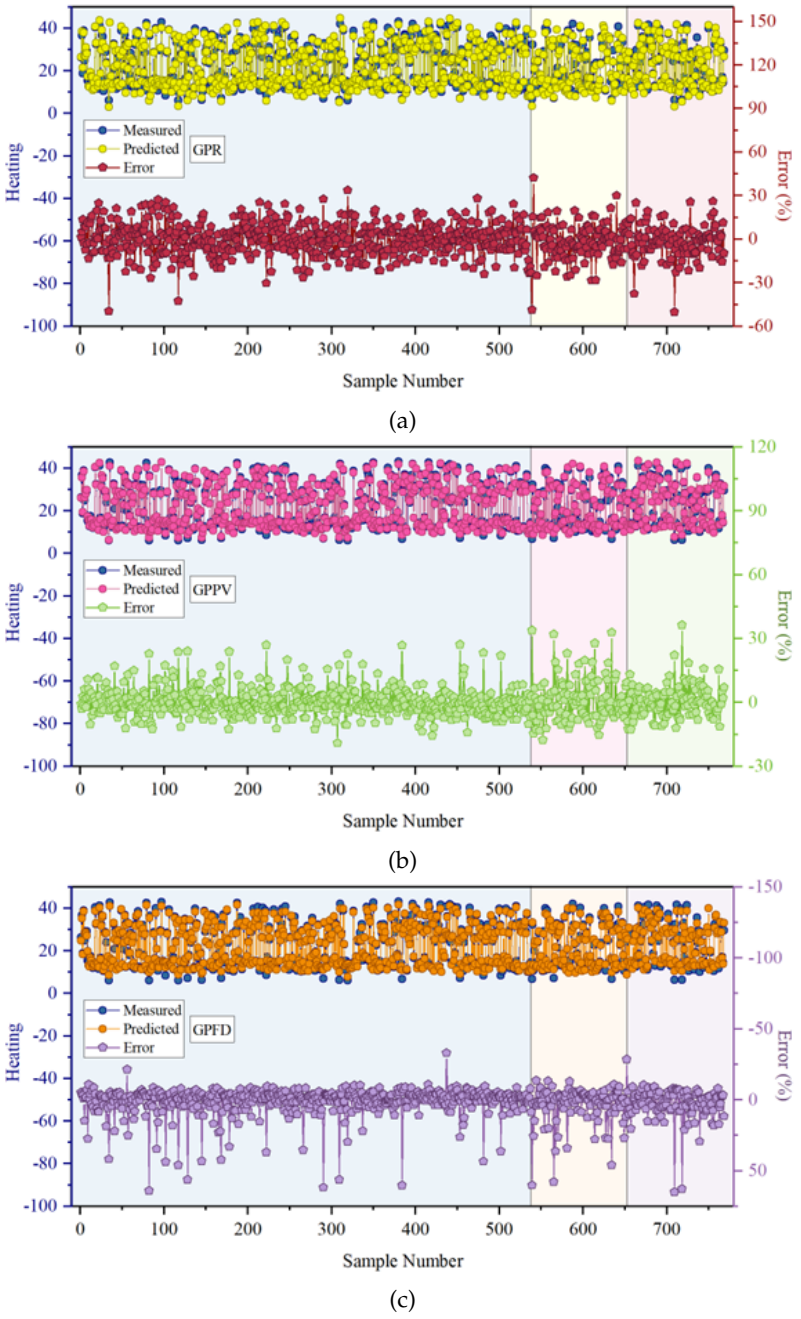

Fig. 2. Error and comparison of measured and predicted for the models based on Line Symbol plot.

shown graphically in Fig. 3 as a scatter interval plot spanning the three separate stages of training, validation, and testing. Interestingly, the GPR model data points show a broad dispersion, spanning error percentages ranging from 50 to -50 . This dispersion is especially noticeable during training. To effectively detect outlier data points for model comparison, a range equal to 1.5 times the Interquartile Range (IQR) is used. On the other hand, the GPPV model data points are noticeably clustered in a very small error percentage range (20 to -20). This suggests that the predictions produced by the GPPV model have a better degree of consistency. However, when compared to the GPR and GPPV models, the GPFD data points show a different distribution pattern, with an error range of 40 to -20 percent.

Fig. 4 shows the Taylor diagram for determining the differences between the predicted and measured values based on standard deviation and correlation coefficient. The ideal

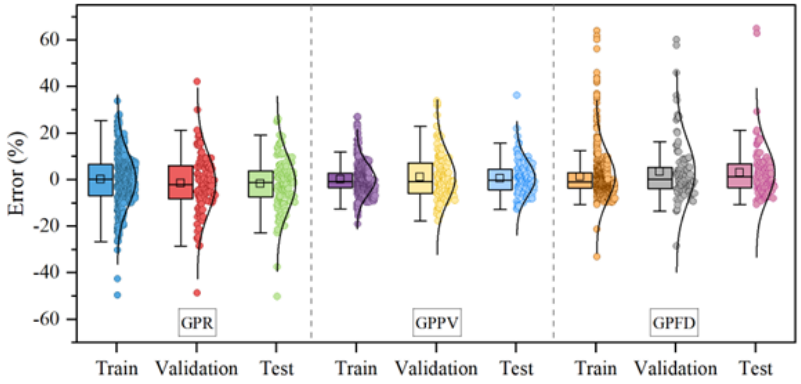

Fig. 3. Box Normal of errors among the developed models.

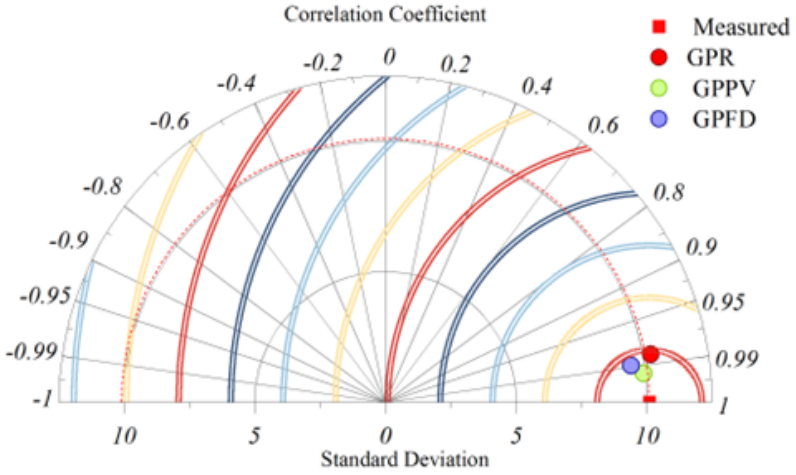

Fig. 4. Taylor diagram for determining the differences between the predicted and measured values.

state for the presented diagram is that the predicted points should be near to measured point. As can be seen, the GPPV obtained the optimal standard deviation and correlation coefficient compared to other models and GPR had the poorest performance.

4.1. Comparison between the presented and published papers

Table 4 highlights the relative strengths and areas for improvement in the present study compared to other published works. The study contributes a novel hybrid approach that achieves a strong balance between accuracy and practical applicability, providing a foundation for further advancements in HL prediction methodologies.

5. Conclusion

In conclusion, this study has provided a comprehensive analysis of estimative models for heating load (HL) in residential buildings, focusing on the performance of the GPR, GPPV, and GPFD models across various phases. The research findings have significant implications for the field of energy management, building efficiency, and sustainability. The GPPV model has consistently demonstrated superior predictive accuracy, maintaining a tight cluster of data points with minimal dispersion throughout the training, validation, and testing phases. This remarkable consistency signifies the GPPV model's reliability in forecasting heating load, making it a valuable tool for energy conser-

Table 4. Comparison of time performance and performance with different superpixel methods

Papers	*Evaluators*	
	RMSE	R^2
Gong et al. [41]	0.193	0.988
Afzal et al. [42]	1.412	0.981
Roy et al. [43]	0.059	0.99
Moradzadeh et al. [44]	0.483	0.999
Present Paper	1.132	0.988

vation and sustainability efforts in residential buildings. Conversely, the GPR and GPFD models displayed wider distributions of error percentages, indicating greater variability in their predictions. These variations, particularly in the GPR model during the training phase, suggest that GPPV's precision sets it apart as a more reliable choice for accurate HL predictions. The visual representations, such as scatter plots and interval plots, have effectively highlighted the distinct distribution patterns of error percentages among the models. These visuals offer clear evidence of the GPPV model's consistent and accurate performance. These findings are not only significant for researchers and professionals in the field of building energy efficiency but also hold substantial practical implications. The GPPV model's precision and reliability make it a valuable asset for optimizing HL prediction, thus contributing to more efficient energy management and reduced environmental impact in residential buildings. As the global emphasis on sustainability and energy conservation continues to grow, the GPPV model's consistently high performance presents an opportunity for real-world applications in enhancing building efficiency and summary, the results of this study underscore the significance of the GPPV model as a promising and accurate tool for predicting HL in residential buildings. Its consistency in performance and precision makes it a standout choice for energy management and sustainability efforts, contributing to the overarching goal of reducing energy waste and minimizing environmental impact. In exploring future works for the proposed forecasting model, avenues for enhancing performance, generalization, scalability, and user-centric applications emerge. Transfer learning and adaptability mechanisms enable the model to generalize across diverse settings and dynamic environments. Scalable cloud-based solutions and integration with smart building systems enhance accessibility and usability. User-friendly interfaces and decision support systems facilitate practical implementation and optimization of energy usage. Sustainability considerations, including carbon footprint reduction and policy recommendations, highlight the model's potential impact on environmental and regulatory landscapes. In summary, future research focuses on refining, generalizing, scaling, and implementing user-centric applications of the forecasting model.

References

[1] Y. Ding, Q. Zhang, T. Yuan, and K. Yang, (2018) *"Model input selection for building heating load prediction: A case study for an office building in Tianjin"* **Energy and Buildings *159***: 254–270. DOI: 10.1016/j.enbuild.2017.11.002.

[2] Y. Shen, *"Load Estimation Models For The Heat Demand Of Buildings: Application Of Optimized Gaussian Process Regression"* **Journal of Applied Science and Engineering *28***(3): 527–541. DOI: 10.6180/jase.202503_28(3).0010.

[3] S. Shamshirband, D. Petković, R. Enayatifar, A. H. Abdullah, D. Marković, M. Lee, and R. Ahmad, (2015) *"Heat load prediction in district heating systems with adaptive neuro-fuzzy method"* **Renewable and Sustainable Energy Reviews *48***: 760–767. DOI: 10.1016/j.rser.2015.04.020.

[4] P. Ming, (2024) *"Hybrid machine learning application with integration of meta-heuristic algorithm for prediction of cooling load"* **Multiscale and Multidisciplinary Modeling, Experiments and Design**: 1–17. DOI: 10.1007/s41939-024-00463-x.

[5] E. Guelpa, L. Marincioni, M. Capone, S. Deputato, and V. Verda, (2019) *"Thermal load prediction in district heating systems"* **Energy *176***: 693–703. DOI: 10.1016/j.energy.2019.04.021.

[6] W. Sun, D. Cheng, W. Peng, et al., (2018) *"Anomaly detection analysis for district heating apartments"* **Journal of Applied Science and Engineering *21***(1): 33–44. DOI: 10.6180/jase.201803_21(1).0005.

[7] Q. Zhang, Z. Tian, Z. Ma, G. Li, Y. Lu, and J. Niu, (2020) *"Development of the heating load prediction model for the residential building of district heating based on model calibration"* **Energy *205***: 117949. DOI: 10.1016/j.energy.2020.117949.

[8] G. Xue, C. Qi, H. Li, X. Kong, and J. Song, (2020) *"Heating load prediction based on attention long short term memory: A case study of Xingtai"* **Energy *203***: 117846. DOI: 10.1016/j.energy.2020.117846.

[9] Y. Zhang, Z. Zhou, J. Liu, and J. Yuan, (2022) *"Data augmentation for improving heating load prediction of heating substation based on TimeGAN"* **Energy *260***: 124919. DOI: 10.1016/j.energy.2022.124919.

[10] J. Zhang, Y. Huang, H. Cheng, H. Chen, L. Xing, and Y. He, (2023) *"Ensemble learning-based approach for residential building heating energy prediction and optimization"* **Journal of Building Engineering *67***: 106051. DOI: 10.1016/j.jobe.2023.106051.

[11] J. Yuan, Z. Zhou, H. Tang, C. Wang, S. Lu, Z. Han, J. Zhang, and Y. Sheng, (2020) *"Identification heat user behavior for improving the accuracy of heating load prediction model based on wireless on-off control system"* **Energy *199***: 117454. DOI: 10.1016/j.energy.2020.117454.

[12] J. Guo, S. Yun, Y. Meng, N. He, D. Ye, Z. Zhao, L. Jia, and L. Yang, (2023) *"Prediction of heating and cooling loads based on light gradient boosting machine algorithms"* **Building and Environment *236***: 110252. DOI: 10.1016/j.buildenv.2023.110252.

[13] G. Xue, Y. Pan, T. Lin, J. Song, C. Qi, and Z. Wang, (2019) *"District heating load prediction algorithm based on feature fusion LSTM model"* **Energies *12***(11): 2122. DOI: 10.3390/en12112122.

[14] F. Dalipi, S. Yildirim Yayilgan, and A. Gebremedhin, (2016) *"Data-Driven Machine-Learning Model in District Heating System for Heat Load Prediction: A Comparison Study"* **Applied Computational Intelligence and Soft Computing *2016***(1): 3403150. DOI: 10.1155/2016/3403150.

[15] J. Ling, N. Dai, J. Xing, and H. Tong, (2021) *"An improved input variable selection method of the data-driven model for building heating load prediction"* **Journal of Building Engineering *44***: 103255. DOI: 10.1016/j.jobe.2021.103255.

[16] E. Küçüktopcu, (2023) *"Comparative analysis of data-driven techniques to predict heating and cooling energy requirements of poultry buildings"* **Buildings *13***(1): 142. DOI: 10.3390/buildings13010142.

[17] C. Wang, J. Yuan, K. Huang, J. Zhang, L. Zheng, Z. Zhou, and Y. Zhang, (2022) *"Research on thermal load prediction of district heating station based on transfer learning"* **Energy *239***: 122309. DOI: 10.1016/j.energy.2021.122309.

[18] R. Chaganti, F. Rustam, T. Daghriri, I. d. l. T. Díez, J. L. V. Mazón, C. L. Rodríguez, and I. Ashraf, (2022) *"Building heating and cooling load prediction using ensemble machine learning model"* **Sensors 22**(19): 7692. DOI: 10.3390/s22197692.

[19] Y. Lu, Z. Tian, Q. Zhang, R. Zhou, and C. Chu, (2021) *"Data augmentation strategy for short-term heating load prediction model of residential building"* **Energy *235***: 121328. DOI: 10.1016/j.energy.2021.121328.

[20] M. Sajjad, S. U. Khan, N. Khan, I. U. Haq, A. Ullah, M. Y. Lee, and S. W. Baik, (2020) *"Towards efficient building designing: Heating and cooling load prediction via multi-output model"* **Sensors *20***(22): 6419. DOI: 10.3390/s20226419.

[21] B. Sadaghat, S. Afzal, and A. J. Khiavi, (2024) *"Residential building energy consumption estimation: a novel ensemble and hybrid machine learning approach"* **Expert Systems with Applications *251***: 123934. DOI: 10.1016/j.eswa.2024.123934.

[22] Z. Wang, T. Hong, and M. A. Piette, (2020) *"Building thermal load prediction through shallow machine learning and deep learning"* **Applied Energy *263***: 114683. DOI: 10.1016/j.apenergy.2020.114683.

[23] B. Sadaghat, A. Javadzade Khiavi, B. Naeim, E. Khajavi, H. Sadaghat, and A. R. Taghavi Khanghah, (2023) *"The utilization of a naive bayes model for predicting the energy consumption of buildings"* **Journal of Artificial Intelligence and System Modelling *1***(01): 73–91. DOI: 10.22034/JAISM.2023.422292.1003.

[24] T.-Y. Kim and S.-B. Cho, (2019) *"Predicting residential energy consumption using CNN-LSTM neural networks"* **Energy *182***: 72–81. DOI: 10.1016/j.energy.2019.05.230.

[25] S. S. Roy, P. Samui, I. Nagtode, H. Jain, V. Shivaramakrishnan, and B. Mohammadi-Ivatloo, (2020) *"Forecasting heating and cooling loads of buildings: A comparative performance analysis"* **Journal of Ambient Intelligence and Humanized Computing *11***: 1253–1264. DOI: 10.1007/s12652-019-01317-y.

[26] A. Moradzadeh, A. Mansour-Saatloo, B. Mohammadi-Ivatloo, and A. Anvari-Moghaddam, (2020) *"Performance evaluation of two machine learning techniques in heating and cooling loads forecasting of residential buildings"* **Applied Sciences *10***(11): 3829. DOI: 10.3390/app10113829.

[27] W. Pessenlehner and A. Mahdavi. *Building morphology, transparence, and energy performance*. Citeseer, 2003.

[28] G. Zhou, H. Moayedi, M. Bahiraei, and Z. Lyu, (2020) *"Employing artificial bee colony and particle swarm techniques for optimizing a neural network in prediction of heating and cooling loads of residential buildings"* **Journal of Cleaner Production *254***: 120082. DOI: 10.1016/j.jclepro.2020.120082.

[29] A. Ghosh, F. Mertens, G. Bernardi, M. G. Santos, N. S. Kern, C. L. Carilli, T. L. Grobler, L. V. Koopmans, D. C. Jacobs, A. Liu, et al., (2020) *"Foreground modelling via Gaussian process regression: an application to HERA data"* **Monthly Notices of the Royal Astronomical Society *495***(3): 2813–2826. DOI: 10.1093/mnras/staa1331.

[30] J. Melo, (2012) *"Gaussian processes for regression: a tutorial"* **Technical Report**:

[31] B. Doğan and T. Ölmez, (2015) *"A new metaheuristic for numerical function optimization: Vortex Search algorithm"* **Information sciences *293***: 125–145. DOI: 10.1016/j.ins.2014.08.053.

[32] J. B. Lindsay, (2003) *"A physically based model for calculating contributing area on hillslopes and along valley bottoms"* **Water Resources Research *39***(12): DOI: 10.1029/2003WR002576.

[33] C. Qin, A.-X. Zhu, T. Pei, B. Li, C. Zhou, and L. Yang, (2007) *"An adaptive approach to selecting a flow-partition exponent for a multiple-flow-direction algorithm"* **International Journal of Geographical Information Science *21***(4): 443–458. DOI: 10.1080/13658810601073240.

[34] C. Depraetere, (1989) *"Etude g6omorphom6trique du bassin-versant de Booro-Borotou• parfir d'un modulen um6fiqued e terrain: Structure et fonctionnement hydrop6dologique d'un petit bassinversant de savane humide; Equipe HYPERBAV, Collection Etudes et Theses, journ• e hydrop• dologique, Inst. Fr. de Rech. Sci. pour le E• vel. en Cooperation"* **Inst. Fr. de Rech. Sci. pour le E• vel. en Cooperation, ORSTOM, Montpellier**:

[35] S. Orlandini, G. Moretti, M. Franchini, B. Aldighieri, and B. Testa, (2003) *"Path-based methods for the determination of nondispersive drainage directions in grid-based digital elevation models"* **Water resources research *39***(6): DOI: 10.1029/2002WR001639.

[36] S. Orlandini and G. Moretti, (2009) *"Determination of surface flow paths from gridded elevation data"* **Water resources research *45***(3): DOI: 10.1029/2008WR007099.

[37] P. Quinn, K. Beven, P. Chevallier, and O. Planchon, (1991) *"The prediction of hillslope flow paths for distributed hydrological modelling using digital terrain models"* **Hydrological processes *5***(1): 59–79. DOI: 10.1002/hyp.3360050106.

[38] T. G. Freeman, (1991) *"Calculating catchment area with divergent flow based on a regular grid"* **Computers & geosciences *17***(3): 413–422. DOI: 10.1016/0098-3004(91)90048-I.

[39] D. G. Tarboton, (1997) *"A new method for the determination of flow directions and upslope areas in grid digital elevation models"* **Water resources research *33***: 309–319. DOI: 10.1029/96WR03137.

[40] A. Botchkarev, (2018) *"Performance metrics (error measures) in machine learning regression, forecasting and prognostics: Properties and typology"* **arXiv preprint arXiv:1809.03006**: DOI: 10.48550/arXiv.1809.03006.

[41] M. Gong, Y. Bai, J. Qin, J. Wang, P. Yang, and S. Wang, (2020) *"Gradient boosting machine for predicting return temperature of district heating system: A case study for residential buildings in Tianjin"* **Journal of Building Engineering *27***: 100950. DOI: 10.1016/j.jobe.2019.100950.

[42] S. Afzal, B. M. Ziapour, A. Shokri, H. Shakibi, and B. Sobhani, (2023) *"Building energy consumption prediction using multilayer perceptron neural network-assisted models; comparison of different optimization algorithms"* **Energy *282***: 128446. DOI: 10.1016/j.energy.2023.128446.

[43] S. S. Roy, P. Samui, I. Nagtode, H. Jain, V. Shivaramakrishnan, and B. Mohammadi-Ivatloo, (2020) *"Forecasting heating and cooling loads of buildings: A comparative performance analysis"* **Journal of Ambient Intelligence and Humanized Computing *11***: 1253–1264. DOI: 10.1007/s12652-019-01317-y.

[44] A. Moradzadeh, A. Mansour-Saatloo, B. Mohammadi-Ivatloo, and A. Anvari-Moghaddam, (2020) *"Performance evaluation of two machine learning techniques in heating and cooling loads forecasting of residential buildings"* **Applied Sciences *10***: 3829. DOI: 10.3390/app10113829.